**Proceedings of ASME 2007 International Design Engineering Technical Conferences &
Computers and Information in Engineering Conference
IDETC/CIE 2007
September 4-7, 2007, Las Vegas, USA**

DETC2007-35751

THE PERFORMANCE EFFECTS OF SQUEEZE FILM STIFFNESS ON NON-RESONATE INTERFEROMETRIC INERTIAL SENSORS

Maximillian A. Perez*
Mechanical and Aerospace Engineering
Email: max.perez@uci.edu
MicroSystems Laboratory
University of California
Irvine, California 92697

Andrei M. Shkel
Mechanical and Aerospace Engineering
Email: ashkel@uci.edu
MicroSystems Laboratory
University of California
Irvine, California 92697

ABSTRACT

This paper studies the nonlinear effects of squeeze film stiffening on the performance of a high resolution MEMS non-resonant inertial sensor. It is shown that these effects introduce a surprising dynamic response that extends the operational frequency range of the devices by retarding the resonate response. In addition, this performance advantage will occur without the traditional gain trade-off associated with linear systems of this type. A method is introduced to experimentally characterize the squeeze film stiffness of a passive inertial sensor through the resonant characterization of a Fabry-Pérot interferometric accelerometer under reduced pressure. Such passive devices are uniquely suited for the study of squeeze films and, due to the dependence of both the sensitivity and bandwidth on the device structural stiffness, variation of the stiffness with frequency must be considered to accurately predict sensor performance. The characterization confirms established analytical squeeze film stiffness theory in the continuous gas regime for conditions of Knudsen numbers less then one. As the Knudsen number equal to one is approached, it is shown that ideal kinetic gas theory and continuous squeeze film theory converge yielding a simplified stiffness estimate at resonance under reduced pressure. These analytical results are used to predict the performance gains due to the nonlinear, frequency dependent total stiffness of the sensor during non-resonant operation.

INTRODUCTION

The characterization of structural parameters is central to the design and performance analysis of inertial sensors employing proof-mass elements. In many Microelectromechanical System (MEMS) devices, the stiffness due to a squeeze film may be a significant component of the total suspension stiffness of such an element. However, in contrast to the stiffness due to flexural suspension members, the squeeze film stiffness is nonlinear and may introduce some surprising dynamic effects.

Squeeze films are formed between closely vibrating surfaces due to the dynamic encapsulation of viscous gases, a representation of such is shown in Figure 1. The earliest description was by Crandell in 1918 [1] for circular plates in parallel motion and a more complete derivation was presented by Langlois in 1962 [2]. Squeeze film effects are commonly encountered in MEMS sensors and actuators due to the small dimensions and the frequent reliance on vibratory motion, such as in micromachined accelerometers [3] and mirrors [4, 5]. For example, squeeze film damping is commonly examined in relation to the quality factor of the amplitude response of resonant devices, as in [6]. Less frequently examined is the effect of squeeze film stiffening on non-resonant sensors. Most prominently, Andrews *et. al* considered the experimental effects of both the damping and stiffness of a squeeze film formed between the square plates of a vibrating microstructure on it's frequency response [7].

The mechanical sensitivity, resolution and usable frequency range (bandwidth) of many non-resonant sensors (such as the

*Address all correspondence to this author.

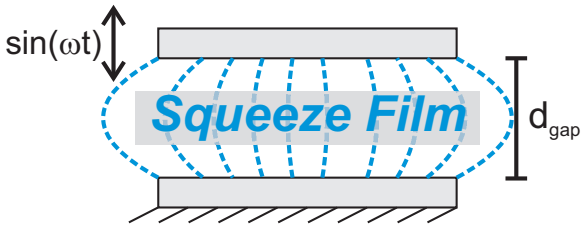

Figure 1. A squeeze film formed between a vibrating and fixed plate

passive accelerometers examined here) is closely related to their structural stiffness. This is due to the dependence of these performance characteristics on the natural frequency of the suspended proof-mass vibrational element composing the sense element of the sensor system. Accurate characterization of this frequency is critical to the understanding of the operating characteristics of the device [8]. Commonly, this characterization is achieved by driving the structure into resonance and deriving the natural frequency from the resonant response. For systems of low damping, these two frequencies are nearly identical. Since for many MEMS structures air damping is the dominant damping source, such characterization is commonly done under vacuum to reduce the damping levels and allow accurate characterization of the natural frequency.

In addition to the evaluation of the structural characteristics at resonance, the mechanical properties of non-resonate accelerometers should be well known over the wide frequency bandwidth below their principle resonance. It is in this region that such instruments are traditionally designed to operate. Since the stiffness properties of a squeeze film are known to be frequency dependent [9], a simple lumped parameter linear modal will not accurately characterize the response over this frequency range.

It is shown in this work that characterization under vacuum allows the proof-mass suspension stiffness contribution due to a squeeze film to be reduced. In this way, the stiffness contribution due to the flexure suspension and the squeeze film may be independently extracted. This allows the mechanical response of the sensor under the operational ambient conditions to be more accurately modeled by considering the frequency dependence of the total proof-mass stiffness over the frequency bandwidth of operation.

BACKGROUND

Knudsen number

Under reduced pressures, the effects of gas rarefaction on behavior of a squeeze film can be characterized by the Knudsen number. The Knudsen number is the ratio of the mean-free-path (λ_m) of a gas particle to the squeeze gap spacing (d_{gas}). For $K_n \ll 1$ the squeeze film is considered to be in the *continuous regime* and can be treated as a viscous fluid. For $K_n \gg 1$ the squeeze film gas can be considered as discrete particles and is said to be in the *free-molecular regime*. The area around $K_n \simeq 1$ is known as the *transition* region [10]. The Knudsen number is calculated as

$$K_n = \frac{\lambda_m}{d_{gap}} = \frac{k_B T}{\sqrt{2}\phi_{gas}^2 P_a d_{gap}}, \tag{1}$$

where k_B is Boltzmann's constant, T is the absolute temperature measured in Kelvin, ϕ_{gas} is the gas molecule diameter, and P_a is the ambient pressure [11]. For example, for a $10\mu m$ gap commonly found in bulk micro-machined structures, the Knudsen number is greater then one for pressures under 2.4kPa (18torr).

The effect of Knudsen number on squeeze film behavior has been previously achieved by replacing a constant gas absolute viscosity (μ) with an Knudsen number dependent *effective* absolute viscosity ($\mu_{eff} = f(K_n)$) in calculations of the properties of a continuous squeeze film. These relationships are empirically derived from experimental data, such as in the work by Veijola *et al.* [12] and Li *et al.* [13]. These relationships become necessary as the unit Knudsen number is traversed and the free-molecular region is entered.

Continuous Squeeze Film Stiffness

For the continuous regime, Blech [9] characterizes the continuous squeeze film by solving the compressible Reynolds equation in terms of the nondimensional squeeze number (σ), given for circular plates as

$$\sigma = \frac{12\mu r^2}{P_a d_{gap}^2}\omega, \tag{2}$$

where ω is the excitation frequency in radian, μ is the gas absolute viscosity, and r is the plate radius. Increasing squeeze number indicates increasing spring force to damping force ratio in a squeeze film.

Adapted from Blech, the squeeze film stiffness for a circular plate is given by

$$k_{cont} = \{1 + \sqrt{\frac{2}{\sigma}}[A_c(ber_1\sqrt{\sigma} + bei_1\sqrt{\sigma}) - B_c(ber_1\sqrt{\sigma} - bei_1\sqrt{\sigma})]\}\frac{P_a A}{d_{gap}}, \tag{3}$$

where A is the area of the plate, P_a is the ambient pressure, and d_{gap} is the gap spacing beneath the plate[1]. Calculation of the

[1]There is a slight error in the formulation of the equation given by Blech in [9] corrected in equation 3 here through comparison with the original work done by Crandall [1]

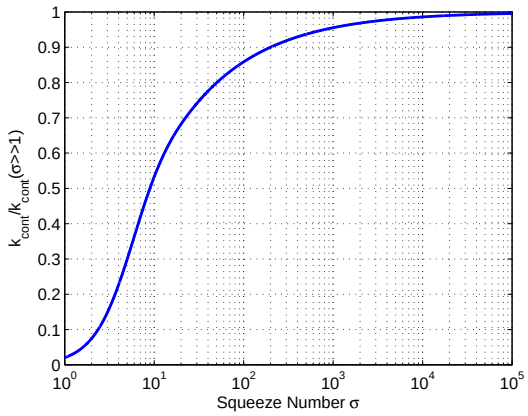

Figure 2. Variation of the normalized squeeze film stiffness with squeeze number σ

Kelvin functions (ber_γ,bei_γ) and the coefficients (A_c,B_c) is described in the Appendix.

It is noted by Andrews *et al.* [7] that in the limit of large squeeze numbers the squeeze film stiffness solutions for square plates given by Blech converges to

$$k_{cont}(\sigma \gg 1) = \frac{P_a A}{d_{gap}}. \tag{4}$$

In this work, it is numerically confirmed that an identical convergence occurs for solution presented by Blech for circular plates, as shown in Figure 2. The convergence is rapid and the error in using equation (4) verses (3) is less then 10% for squeeze numbers greater then 200. In addition, for constricted boundary conditions (increased pressure at the edge of the squeeze film due to non-ideal venting geometry), the problem may solved by superposition and the convergence has been shown to occur more rapidly [14].

For any particular device operating under fixed pressure conditions, large squeeze numbers are achieved at higher frequencies. For the non-resonate sensors considered here, the upper end of the frequency range is limited by the resonant response. Under these conditions, large squeeze number are frequently experienced and the quantity given by (4) may be used to estimate the stiffness due to a squeeze film at resonance in many instances.

Ideal Pressure Spring

Insight into equation (4) may be gained by modeling the enclosed gas particles in the squeeze film as discrete particles, as in Figure 3. Basic kinetic theory predicts the relation between the pressure on a surface and kinetic energy of the surrounding gas particles. A well known result for an enclosed volume (V) is that

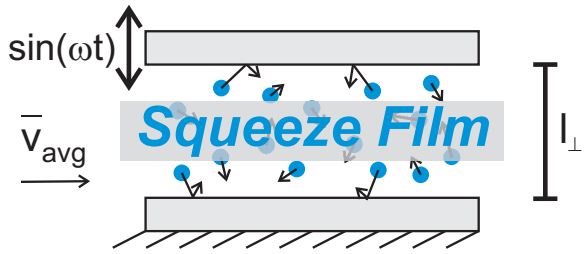

Figure 3. The discrete particles of the gas forming a squeeze film each with average velocity $\overline{v_{avg}}$ contained in a cavity between plates of perpendicular separation $l_\perp$

the force on one surface (F_{surf}) of the volume is given by

$$F_{surf} = \frac{N m_{gas} \overline{v_\perp^2}}{l_\perp}, \tag{5}$$

where N is the number of particles in the volume, m_{gas} is the mass of each gas particle, $\overline{v_\perp}$ is the average velocity of the enclosed gas particles perpendicular to the surface and $l_\perp$ is the dimension of the volume perpendicular to the surface. [15]

Applying Hooks law ($k = -\frac{dF}{dx}$), the stiffness of the enclosed volume (k_{vol}) under perpendicular (x) displacement of the plate is given as

$$k_{vol} = \frac{N m_{gas} \overline{v_\perp}^2}{l_\perp^2}. \tag{6}$$

Applying the ideal gas law ($P_a V = N k_B T$) and the velocity due to the thermal excitation of a particle ($\overline{v_\perp}^2 = k_B T / m_{gas}$) to (6) yields

$$k_{vol} = \frac{P_a V}{l_\perp^2} = \frac{P_a A}{d_{gap}}, \tag{7}$$

which is identical to (4) when the surface displacement is perpendicular and $l_\perp = d_{gap}$. This identity indicates the connection between the continuous and molecular regimes. From this, we may make the observation that under high squeeze number conditions we expect the continuous squeeze film to act like a perfectly enclosed volume of an ideal gas or a perfect *pressure spring*.

Although this analysis considers the molecules of the squeeze film gas as individual particles, the ideal gas assumptions used imply that the gas interact most frequently with each other and little energy is exchanged with the vibrating plate. Such assumptions would be expected to be valid up to the limit of the Knudsen number equal to one ($K_n = 1$). Once the unit

Knudsen number is traversed, the transition to the free molecular regime is entered and the gas molecules will contact the surfaces more frequently then each other and ideal gas assumptions may not be valid. In such regimes, it may be necessary to consider the energy gain in the squeeze film due to momentum exchange between individual molecules and the vibrating plate element [10, 16].

Comparing the limits of the two approaches, the application of (4) and (7) can be limited to a specific range of conditions. From the continuous film derivation, the simplified expression holds true only under conditions in which large squeeze numbers (large gap aspect ratios (r/d_{gap}), reduced pressures, or high excitation frequencies) are experienced. From the discrete molecule model, the expression holds only when Knudsen numbers less then one (relatively high pressures) are experienced. Thus, characterization of squeeze film stiffness from the resonant characteristics of microstructures is most readily done under moderately reduced pressure but not high vacuum. This is true for many micromachined devices, including the sensors characterized here.

EXPERIMENTAL

The squeeze film stiffness characteristics of passive seismic proof-mass micromachined vibrometers based on parallel plate Fabry-Pérot interferometers (FPI) are characterized (Figure 4a). The optical characteristics of these device require geometries (high gap aspect ratios, smooth surfaces, no perforations) that show substantial squeeze film characteristics. The devices are formed from pairs of micromachined substrates (Figure 4b) with mirrored surfaces micro-assembled to form parallel faces with a gap controlled by a spacer and fixed with epoxy. The *proof-mass mirror substrate* is composed of 'thinned-wafer' flexure connecting the proof-mass to a frame. The *reference mirror substrate* contains a similar structure where the flexure has been replaced by fixed supports to minimize compliance (Figure 5a).

Mechanical Response

Under base displacement $y(t)$, the Laplace domain (s) transfer function sensor is given by

$$\frac{Z(s)}{Y(s)} = \frac{-ms^2}{ms^2 + c_{sf}s + k_{tot}}, \tag{8}$$

where m is is the mass of the proof mass, c_{sf} is the damping attributable to the squeeze film, and k_{tot} is the total structural stiffness composed of the components due to the squeeze film k_{sf} and the flexure suspension k, such that $k_{tot} = k_{sf} + k$. (Fig 5b) When normalized by mass, the parametric model is expressed as

$$\frac{Z(s)}{Y(s)} = \frac{-s^2}{s^2 + 2\omega_n\zeta s + \omega_n^2}, \tag{9}$$

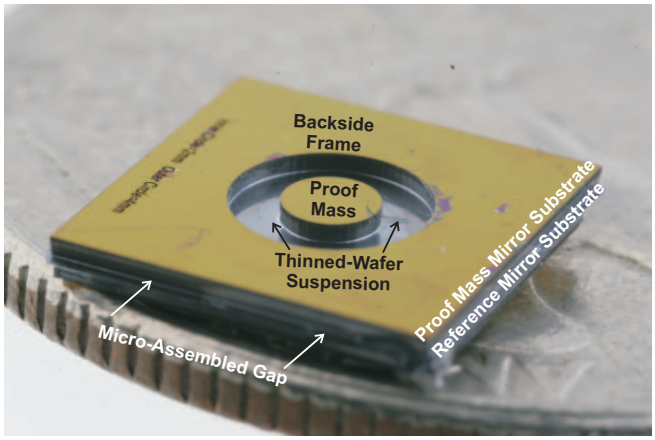

(a) Micro-assembled FPI-based inertial sensor (located on a quarter for scale

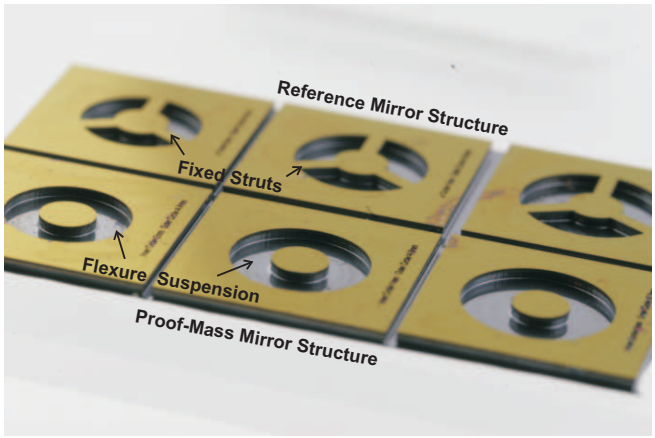

(b) An array of pairs of micromachined FPI-based accelerometer components

Figure 4.

where the angular natural frequency $\omega_n = \sqrt{k_{tot}/m}$ and the damping ratio $\zeta = c_{sf}/2m\omega_n$.

Opto-mechanial Response

The operation of the FPI-based inertial sensor has been explained in depth previously. [17, 18] Briefly, the spectral position of an interferometric fringe created by an optical cavity between two reflective surfaces allows the cavity spacing to be closely monitored. If one surface is the face of a proof mass and the other of an inertial reference, the deflection between the plates (z) is related to the displacement of the reference plate (y) with a proportional shift in the fringe position and is governed by

$$y = \left[\frac{Y(s)}{Z(s)}\right]_{s=i\omega} \frac{n(\lambda - \lambda_i)}{2}, \tag{10}$$

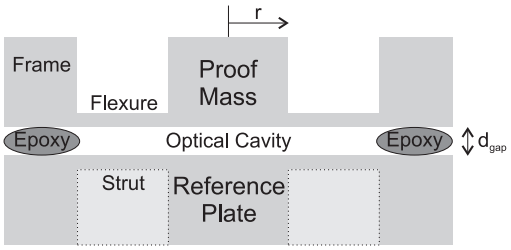

(a) Cross-section of the assembled device

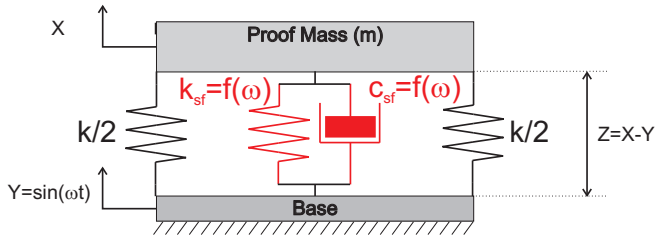

(b) Lumped parameter model of the passive accelerometer structure with flexure suspension stiffness (k), squeeze film stiffness (k_{sf}) and damping (c_{sf}) under sinusoidal base excitation $y(t)$ of frequency ω

Figure 5.

where n is the optical order of the FPI, λ_i is the initial (resting) wavelength position of the fringe, and λ is the wavelength position of the fringe under acceleration a. If the 'shoulder' of the fringe is monitored at a particular wavelength, as with a laser, the response of the sensor is given as

$$y = \underbrace{\left[\frac{Y(s)}{Z(s)}\right]_{s=i\omega}}_{\text{MECHANICAL}} \underbrace{\frac{n}{2}\left[\frac{\delta\lambda}{\delta T}\right]_{\lambda_0}}_{\text{OPTICAL}} \frac{1}{P_{\lambda_0}} \Delta P, \qquad (11)$$

where $[\delta T/\delta\lambda]_{\lambda_0}$ is the slope of the fringe, P_{λ_0} is steady-state optical power transmitted at the operating wavelength λ_0 and ΔP is the change in transmitted optical power under excitation, where the mechanical and optical components of the response have been labeled. Using (11), the base displacement is monitored as a modulation in the optical power transmitted through the device at a particular wavelength. In this work, we are concerned with the mechanical characteristics of the sensor and consider the optical characteristics as constant. In this work λ_o is chosen to be at the midpoint or *half-maximum* of the fringe to maximize $[\delta T/\delta\lambda]_{\lambda_0}$ over the greatest range.

Experimental Stage

In order to provide swept frequency excitation to the FPI-based sensor, an excitation stage was developed that could both vertically excite the sensor sample and provide optical access through the bulk of the sample. A cylindrical piezoelectric stack

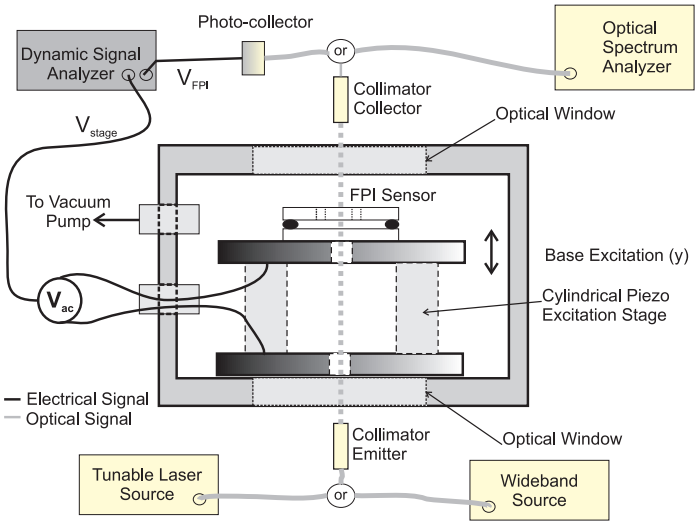

Figure 6. Experimental stage setup for base-excitation of FPI sensor with pressure variation

was acquired (Steiner & Martins - SMR2412T80) to provide excitation. The electromechanical resonant frequency of the piezoelectric stack ($\simeq 60kHz$) was chosen to be greater then the range of frequencies of the tests to prevent the introduction of resonant modes from the actuator. Two electrical leads were soldered to the top and bottom surfaces of the stack. Up to 50 V_{AC} was used to excite vertical deformation in the stack providing base excitation to the sample. This stage was inserted into a vacuum chamber under which the pressure could be varied from less then 1 torr (133 Pa) to atmospheric pressure. Two collinear optical windows were installed on the stage to provide optical access through the stage, the excitor and the sample. A pigtailed collimated fiber was connected to the optical source and used as an emitter to provide the pick-off signal to the sample. A similar collimated fiber was aligned collinear with the emitter to collect the optical signal.

Both laser and broadband sources were used with this stage: the first for the static optical characterization of the device and the second for the dynamic characterization. When the tunable laser source (HP 8168E) was used, the optical collector was coupled to a photo-collector (Thorlabs PDA255) that sampled the optical power of the transmitted signal. The voltage signal from the photo-collector was then acquired by a dynamic signal analyzer (HP 35665A).

The piezo-excitation voltage was controlled by the dynamic signal analyzer such that during swept sign analysis the sample response voltage modulation was kept constant to within 1dB of variation. This ensures that under excitation (a) the fringe shift is small in comparison to the fringe width (FWHM) and the optical properties of $[\delta T/\delta\lambda]_{\lambda_0}$ can be considered as constant and (b) the proof mass deflection has a constant excited amplitude throughout the test. Since the voltage applied to the piezo-stack

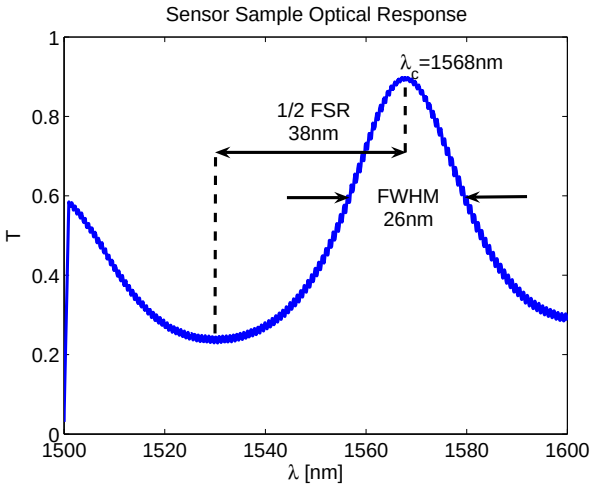

Figure 7. Optical **T**ransmittance characterization of the sample indicating half the free spectral range (FSR) and full-width at half maximum (FWHM)

stage (V_{stage}) is proportional to the base displacement y and the voltage from the photo-collector (V_{FPI}) is proportional to the FPI response due to the proof-mass displacement z, the frequency response can evaluated by $\left[\frac{Z(s)}{Y(s)}\right] \propto \frac{V_{FPI}}{V_{Stage}}$.

Optical Characterization

The close relationship between gap spacing and the optical characteristics that provides the device with its sensing mechanism also provides gap characterization precision not readily available in other micromachined structures. Figure 7 shows the static optical characteristics of the tested sample. From the well established characteristics of the parallel plate Fabry-Pérot interferometer, the order $n = \lambda_c/FSR = 21$, the FPI resolution or *finesse* $N = \frac{FSR}{FWHM} \simeq 3$, and in air the cavity gap $d_{gap} = n\lambda_c/2 = 16.5\mu m$ [19]. Thus, the squeeze film gap aspect ratio is $r/d_{gap} = 60$. The fringe slope at λ_o at the half-maximum can be characterized directly as from figure 7 and is $[\delta T/\delta\lambda]_{\lambda_0} = 0.05nm^{-1}$.

The fringe was limited to shifts of $\simeq 0.2nm$. From the optical sensitivity of the device and the control voltage, an maximum excitation amplitude of $\pm 22pm$ ($\pm 22 \cdot 10^{-12}m$) is determined. For the nominal $d_{gap} = 17\mu m$, a total deflection of $\simeq \pm 0.1\%$ of the gap was maintained throughout the excitation tests.

Experimental Results

The frequency response of a number of FPI-based accelerometers were obtained. For example, Figure 8 shows the frequency response of a device under base-displacement excitation. Note the general shift to higher resonant frequencies as the pressure is increased indicative of squeeze film stiffening. In-

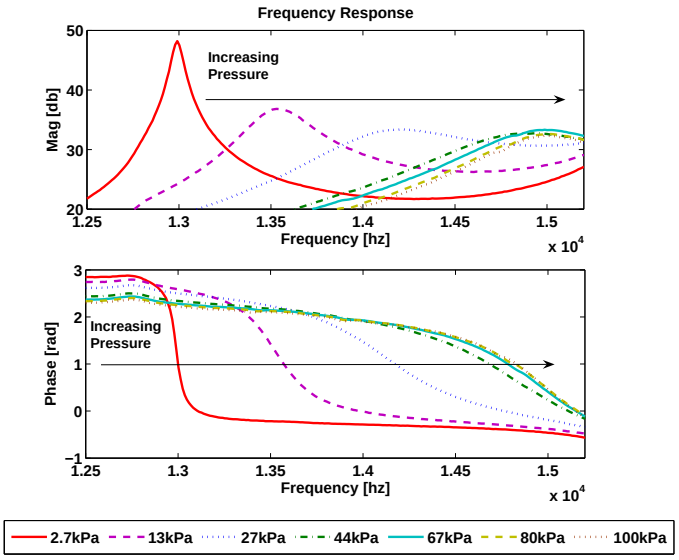

Figure 8. Frequency response at resonance of a FPI-based vibrometer at various pressures

creased damping associated with the squeeze film is noted in response peak broadening with pressure. The phase response of the device yields a measure of the undamped natural frequency ($f_n = \omega_n/2\pi$) of the device by calculating the $\pi/2$ phase shift cross-over according to

$$f_n = \sqrt{f_{\frac{\pi}{4}} f_{\frac{3\pi}{4}}}, \tag{12}$$

where $f_{\frac{\pi}{4}}$ and $f_{\frac{3\pi}{4}}$ are the frequencies of the $\frac{\pi}{4}$ and $\frac{3\pi}{4}$ phase shift points. [20]

Using (12), the natural frequencies are extracted. From the definition of natural frequency, the mass normalized squeeze film stiffness is calculated from each frequency response curve according to

$$\frac{k_{sf}}{m} = \omega_n^2 - \frac{k}{m}. \tag{13}$$

The proof mass (m) is readily estimated from the sensor geometry. The normalized flexure stiffness is $k/m = (2\pi f_n)^2$, where f_n is calculated according to (12) from the resonant response under the lowest available pressure.

Using the preceding technique, Figure 9 shows the response of the squeeze film stiffness versus that predicted by the theoretical expression presented previously in (3) and (4). In order to approximate the response from nonideal venting conditions the squeeze number was scaled by a factor of ten to match the experimental data. One can identify two regions of interest in the

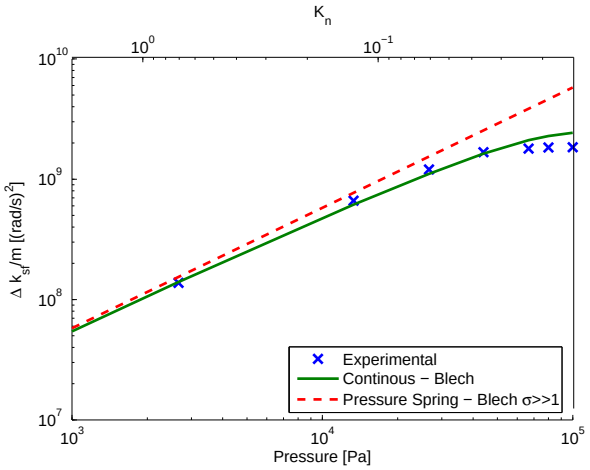

Figure 9. Calculation of the mass-normalized squeeze film stiffness for the data of figure 8 relative to Knudsen number (K_n) and pressure

response. At high pressure and low Knudsen number, the continuous theory presented by Blech accurately predicts the features of the response. As the squeeze number increases and the Knudsen number approaches one from the left-hand side, the behavior can be predicted by the ideal pressure spring response of (4) and (7).

DISCUSSION

Accelerometer Performance

Multiplying (9) by $1/s^2$ yields the mechanical response of the FPI-based vibrometer under base acceleration A_y as

$$\frac{Z(s)}{A_y(s)} = \frac{-1}{s^2 + 2\omega_n\zeta s + \omega_n^2}. \tag{14}$$

Passive vibrometers are used as non-resonate accelerometers at frequencies in the flat, gain stable frequency response region below their natural frequency (ω_n). This is done in order to maintain a constant response across all the detected frequencies. The extent of this region is known as the mechanical or open-loop *sensor bandwidth*. From (14) as $s \to 0$, non-resonate accelerometers have the low-frequency response or *DC gain*

$$\frac{z}{a_y} = -\frac{1}{\omega_n^2}. \tag{15}$$

Using (15), from (11) the FPI-based accelerometer response is

$$a = -\omega_n^2 \frac{n}{2}\left[\frac{\delta\lambda}{\delta T}\right]_{\lambda_0} \frac{1}{P_{\lambda_0}}\Delta P, \tag{16}$$

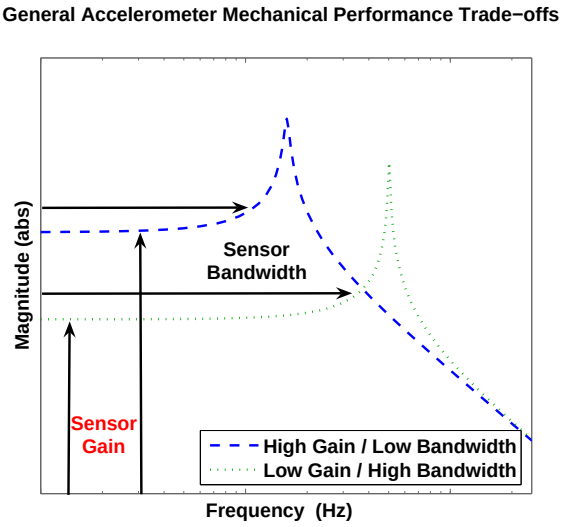

Figure 10. General performance trade-offs of accelerometers with constant lumped parameters and linear response characteristics

such that increasing the sensor's natural frequency decreases the gain and reduces the acceleration sensitivity.

For systems with subcritical, nonzero damping levels ($0 < \zeta < 1$), (15) is generally valid within one dB of linearity for the frequency band up to one-third of the natural frequency [8]. For lumped parameter estimation, the operational sensor bandwidth is proportional to natural frequency and can be estimated as

$$\Delta f_{BW} \simeq \frac{1}{3}\frac{\omega_n}{2\pi}. \tag{17}$$

For such sensors as the natural frequency is increased to increase the bandwidth, the gain of the device is necessarily reduced. Thus, a fundamental trade-off between sensitivity and bandwidth is observed in passive accelerometers. Figure 10 shows the response of an ideal accelerometer according to the linear model (9) for both a high and low natural frequency frequency suspended proof-mass accelerometer illustrating these trade-offs.

Squeeze Film Effect on Frequency Response

The natural frequency and the damping ratio are readily evaluated from the resonate response of the device. Assuming a lumped parameter model, the accelerometer response can be evaluated from the response according to (14). The bandwidth and gain of the sensor can be estimated from this response.

However, it has been shown that squeeze films have properties which are strongly frequency dependent. At any given operating conditions, the squeeze number will vary linearly with

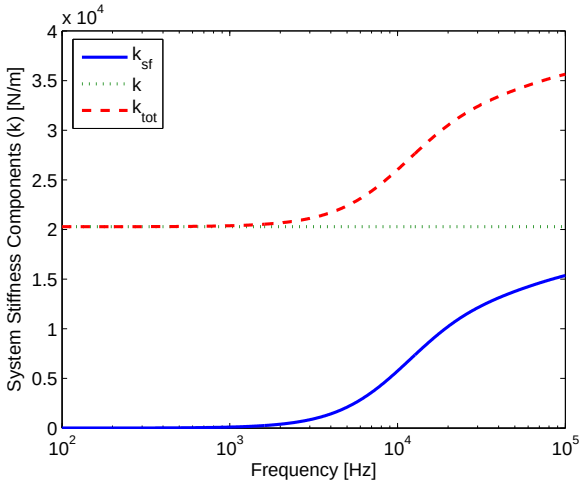

Figure 11. Calculated shift in the components and total proof mass suspension stiffness due to frequency dependence of squeeze films for the experimental characterization shown in Figures 8 and 9

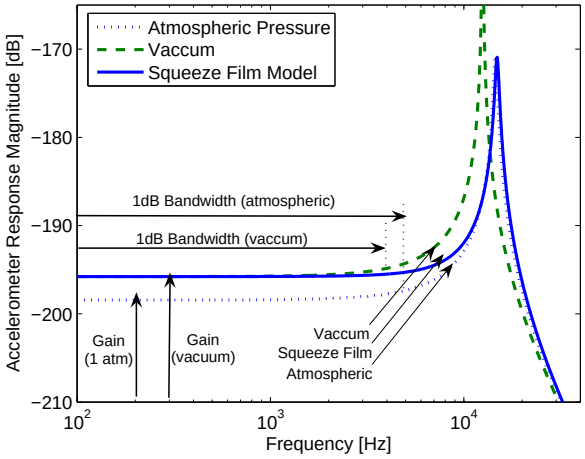

Figure 12. The analytically estimated mechanical response of the accelerometer under the properties calculated from the experimental characterization from Figures 8 and 9

excitation frequency ω and the squeeze film stiffness will vary according to (3), as shown in Figure 2. Accordingly, system with strong squeeze film characteristics will not be accurately modeled by the lumped parameters evaluated at the resonate frequency. Due to the dependence of both the sensitivity and bandwidth of such sensors on the device structural stiffness, variation of the stiffness with frequency must be considered to accurately predict sensor performance. Only by accurately identifying the frequency independent (k) and frequency dependent (k_{sf}) components of stiffness, the total stiffness (k_{tot}) can be correctly calculated and the sensitivity and bandwidth can be accurately modeled.

Figure 11 shows the characteristics increase of the stiffness with frequency for the system with parameters extracted from figure 8. The frequency independent (k) component of stiffness is calculated from the response at the lowest available pressure. The squeeze film component (k_{sf}) is calculated from the continuous squeeze film stiffness relationship of (3). The total stiffness is the sum of the two, $k_{tot} = k + k_{sf}(\omega)$.

The linear model of (8) is used to evaluate the response under these nonlinear stiffness characteristics. This model is evaluated for k_{tot} calculated for each frequency ω in the range and used to calculate the magnitude response at that excitation frequency. At each individual frequency excitation, a constant k_{tot} is assumed. The linear model of (14) is then used to estimate the frequency response at that frequency and this estimation is completed at each of the frequencies in the range. In this way the nonlinear, frequency dependent response is estimated using the linear model according to the known frequency dependence of the squeeze film.

The results of the nonlinear response (*squeeze film*) estimation of the FPI-based vibrometer to acceleration input are shown in Figure 12. Also shown are the responses according to the linear model for the the properties of the response under *vacuum* and *one atmosphere*. These are estimated using the lumped parameters calculated from the experimental resonate responses of figure 8 obtained under the lowest available pressure and atmospheric pressure[2]. Since the frequency dependance of the stiffness characteristics are included, the squeeze film response shows a more accurate characterization of the sensor response in ambient conditions then that estimated from an estimation of the lumped parameters from a single resonate response.

Bandwidth and Gain Trade-off

For the lumped parameter estimates, the following is observed. The response under vacuum has a mechanical gain $2.7dB$ over that of the response under atmospheric pressure. However, the bandwidth (less then $1dB$ amplitude response variation) under low vacuum is limited to $\sim 1kHz$ less then that of the atmospheric response. Significantly, the nonlinear (squeeze film) response characteristics show neither trade-off and shows the higher performance advantages associated with both of the linear models.

Since the squeeze film stiffness is insignificant at lower frequencies within the sensor bandwidth, the actual response retains high gain characteristics identical to that of the response at low vacuum. As the frequency increases, the squeeze film stiffness increases and becomes a larger component of the total system stiffness. This retards the resonant response relative to frequency and increased the flat frequency response region used for the

[2]Estimation of the natural frequency from the resonant response was done from the phase response according to (12). Estimation of damping ratio was done using half-power points [21].

sensor bandwidth. Thus, the characteristic gain and bandwidth performance trade-off in non-resonant accelerometers can be reduced by the use of structures that have a high level of squeeze film stiffening. Such an effect may be used to extend the bandwidth of non-resonant sensors without sacrificing gain by maximizing squeeze film stiffness in device design.

For the sensor characterized here, we observe a dynamic performance trade-off between a 15% loss in bandwidth for the low pressure response in which the squeeze film stiffness has been eliminated versus a 27% loss in mechanical sensitivity due to the shift to a higher natural frequency under the the atmospheric response. By both decreasing the low frequency stiffness and elongating the flat frequency response region by retarding the resonant response, the ambient response shows that the performance with a squeeze film eliminates both these performance losses.

CONCLUSIONS

This paper characterizes the nonlinear effects of squeeze film stiffening on the performance of a high performance MEMS non-resonant inertial sensor. It is shown that such effects will extend the operational frequency range of the devices by retarding the resonate response that usually limits the sensing bandwidth. In addition, this performance increase will occur without the traditional gain trade-off associated with linear systems of this type. This is due to the frequency dependence of squeeze film stiffness due to strengthening operation at higher frequencies. Employing a unique vacuum micro-vibration stage with optical ports and using resonant vibration testing methods, the squeeze film stiffness of this device is extracted. The squeeze film stiffness under varying pressure is compared to established analytical models. The connection between these models and kinetic gas theory is established to confirm the results under the Knudsen numbers (sparse gas) conditions approached in these devices. When compared to linear models normally employed to describe such systems, it is experimentally observed that the dynamic performance trade-off as high as a 15% loss in frequency bandwidth versus a 27% loss in mechanical sensitivity is largely eliminated with the inclusion of nonlinear squeeze film stiffness effects.

ACKNOWLEDGMENT

This work is supported in part by the NSF Grant CMS-0223050. The authors further wish to acknowledge the staff of the INRF for assistance with sample fabrication, Polytec USA for assistance with dynamic sample characterization and colleges Adam Schofield for help with figure preparation and Alex Trusov for motivating discussion.

REFERENCES

[1] Crandall., I. B., 1918. "The air-damped vibrating system: Theoretical calibration of the condenser transmitter". *Phys. Rev.,* **11**(6), Jun, pp. 449–460.

[2] Langlois, W., 1961. "Isothermal squeeze films". *Quarterly of Applied Math,* **XX**(2), pp. 131–150.

[3] Starr, J. B., 1990. "Squeeze-film damping in solid-state accelerometers". In 4th Tech. Digest IEEE Solid State Sensor and Actuator Workshop (Hilton Head Island, SC, 1990), pp. 44–47.

[4] Pan, F., Kubby, J., Peeters, E., Tran, A. T., and Mukherjee, S., 1998. "Squeeze film damping effect on the dynamic response of a mems torsion mirror". *Journal of Micromechanics and Microengineering,* **8**, September, pp. 200–208.

[5] Chang, K.-M., Lee, S.-C., and Li, S.-H., 2002. "Squeeze film damping effect on a mems torsion mirror". *Journal of Micromechanics and Microengineering,* **12**, September, p. 556.

[6] Cheng, C.-C., and Fang, W., 2003. "Tuning the quality factor of bulk micromachined structures using the squeeze film damping". In 12th International Conference on TRANSDUCERS, Solid-State Sensors, Actuators and Microsystems, Vol. 2, pp. 1590– 1593.

[7] Andrews, M., Harris, I., and Turner, G., 1991. "A comparison of squeeze-film theory with measurements on a microstructure". *Sensors and Actuators A,* **36**, pp. 79–87.

[8] Eren, H., 2000. *Measurement, Instrumentation, and Sensors Handbook*. CRC Press LLC, ch. 17 Acceleration, Vibration, and Shock Measurement.

[9] Blech, J., 1982. "On isothermal squeeze films". *Journal of Lubrication Technology,* **105**, pp. 615–620.

[10] Hutcherson, S., and Ye, W., 2004. "On the squeeze-film damping of micro-resonators in the free-molecule regime". *Journal of Micromechanics and Microengineering,* **14**(12), pp. 1726–1733.

[11] Minikes, A., Bucher, I., and Avivi, G., 2005. "Damping of a micro-resonator torsion mirror in rarefied gas ambient". *Journal of Micromechanics and Microengineering,* **15**(9), pp. 1762–1769.

[12] Veijola, T., Kuisma, H., Lahdenpera, J., and Ryhanen, T., 1995. "Equivalent-circuit model of the squeezed gas film in a silicon accelerometer". *Sensors and Actuators A: Physical,* **48**(3), May, pp. 239–248.

[13] Li, G. X., and Hughes, H. G., 200. "Review of viscous damping in micromachined structure". *Proc. SPIE,* **4176**, August, pp. 30–46.

[14] Darling, R., and Yang, J., 1997. "Compact analytical models for squeeze film damping with arbitrary venting conditions". In TRANSDUCERS '97 International Conference on Solid State Sensors and Actuators, Vol. 2, pp. 1113–1116.

[15] Resnick, R., Halliday, D., and Krane, K., 1992. *Physics*,

Vol. 1. John Wiley and Sons, Inc.
[16] Bao, M., Yang, H., Yin, H., and Sun, Y., 2002. "Energy transfer model for squeeze-film air damping in low vacuum". *Journal of Micromechanics and Microengineering,* **12**(3), pp. 341–346.
[17] Yoshino, T., Kurosawa, K., Itoh, K., and Ose, T., 1982. "Fiber-optic fabry-perot interferometer and its sensor applications". *IEEE Transactions on Microwave Theory and Techniques,* **82**(10), Oct, pp. 1612–1621.
[18] Udd, E., 1996. "Fiber optic smart structures". *Proceedings of the IEEE,* **84**(6), June, pp. 884–894.
[19] Atherton, P. D., Reay, N. K., Ring, J., and Hicks, T. R., 1981. "Tunable Fabry-Perot filters". *Optical Engineering,* **20**(6), pp. 806–814.
[20] IEEE, 1998. *IEEE standard specification format guide and test procedure for linear, single-axis, nongyroscopic accelerometers*, std 1293-1998 ed.
[21] Rao, S. S., 1995. *Mechanical Vibrations*, Vol. 3. Addison-Wesley.

Appendix

The Kelvin functions *ber* and *bei* are given by

$$ber_\gamma(x) + ibei_\gamma(x) = J_\gamma(xe^{3\pi i/4}) \tag{18}$$

where $J_\gamma()$ is a Bessel function of the first kind.

The coefficients of (3), A_c and B_c, are given as

$$A_c = \frac{bei\sqrt{\sigma}}{ber^2\sqrt{\sigma} + bei^2\sqrt{\sigma}} \tag{19}$$

$$B_c = -\frac{ber\sqrt{\sigma}}{ber^2\sqrt{\sigma} + bei^2\sqrt{\sigma}} \tag{20}$$